Cell Calcium 54 (2013) 343–349

Contents lists available at ScienceDirect

Cell Calcium

journal homepage: www.elsevier.com/locate/ceca

Subcellular location of astrocytic calcium stores favors extrasynaptic neuron–astrocyte communication

Ilya Patrushev[a,1], Nikolay Gavrilov[b,1], Vadim Turlapov[b], Alexey Semyanov[a,b,*]

[a] RIKEN Brain Science Institute, Wako, Saitama, 351-0198, Japan
[b] University of Nizhny Novgorod, Nizhny Novgorod, Russia

ARTICLE INFO

Article history:
Received 7 August 2013
Received in revised form 14 August 2013
Accepted 17 August 2013
Available online 28 August 2013

Keywords:
Astrocyte
Postsynaptic density
Perisynaptic processes
Neuron–glia interaction

ABSTRACT

Neuron–astrocyte interactions are important for brain computations and synaptic plasticity. Perisynaptic astrocytic processes (PAPs) contain a high density of transporters that are responsible for neurotransmitter clearance. Metabotropic glutamate receptors are thought to trigger Ca^{2+} release from Ca^{2+} stores in PAPs in response to synaptic activity. Our ultrastructural study revealed that PAPs are actually devoid of Ca^{2+} stores and have a high surface-to-volume ratio favorable for uptake. Astrocytic processes containing Ca^{2+} stores were located further away from the synapses and could therefore respond to changes in ambient glutamate. Thus, the anatomic data do not support communication involving Ca^{2+} stores in tripartite synapses, but rather point to extrasynaptic communication.

1. Introduction

Astrocytes are responsible for glutamate uptake around the synaptic cleft [1,2], thus limiting synaptic neurotransmitter escape [3] and the diffusion of ambient glutamate into the synaptic cleft [4,5]. These cells are also responsible for the clearance of K^+ that becomes elevated during action potentials and synaptic transmission (e.g., through AMPA and NMDA receptors) [6–8]. Thus, the spatial relationship between synapses and astrocytes is critical for both glutamate uptake and K^+ clearance. Astrocytic processes tend to locate close to synapses. For example, 64–90% of synaptic clefts in the hippocampus are sealed by astrocytic processes [9], which is significantly more than expected from random positioning of astrocytes in tissue with a 4–33% volume of glial cell processes. The anatomic and functional relationship between astrocytic processes and synaptic clefts led to the idea of tripartite synapses, in which astrocytes are an important functional component in addition to presynaptic axonal boutons and postsynaptic spines [10,11]. Notably, the coverage of the synapse by PAPs changes under different physiologic conditions and is regulated by the Ca^{2+} dynamics in the astrocytes [12,13].

In addition to effective glutamate uptake and K^+ clearance, the idea of tripartite synapses is linked to receptor-mediated neuron–astrocyte communication. Astrocytes express various receptors for synaptically released neurotransmitters and thus potentially respond to synaptic activity [14]. A typical example is astrocytic metabotropic glutamate receptors, which are activated by synaptically released glutamate and trigger astrocytic Ca^{2+} responses [15–17]. Such Ca^{2+} events are mediated by IP_3 receptor (IP_3R)-dependent Ca^{2+} release from intracellular Ca^{2+} stores (e.g., endoplasmic reticulum and mitochondria) [18,19]. The presence of Ca^{2+} stores in astrocytic processes is required for the generation of such events. Surprisingly, many PAPs appear 'empty' (i.e., without organelles) in electron microscope images, suggesting that they may not be able to generate Ca^{2+} events in response to metabotropic glutamate receptor activation [20]. The location of 'active' (containing Ca^{2+} stores) versus 'inactive' (devoid of Ca^{2+} stores) astrocytic processes around the synaptic cleft, however, has not been systematically studied. Therefore, in the present study, we performed three-dimensional (3D) reconstructions of electron microscope serial sections of astrocytic processes to analyze the correlation between the Ca^{2+} dynamics and the presence of Ca^{2+} stores.

2. Methods

2.1. Animals and tissue preparation for electron microscopy

Male Wistar rats weighing 250 ± 25 g were deeply anesthetized with sodium pentobarbital (100 mg/kg, i.p.) then perfused transcardially with 100 ml of physiologic saline, followed by 100–150 ml of 3% paraformaldehyde and 0.5% glutaraldehyde in

* Corresponding author at: RIKEN Brain Science Institute (BSI), 2-1 Hirosawa, Wako-shi, Saitama 351-0198, Japan. Tel.: +81 48 467 6924; fax: +81 48 467 9652.
E-mail address: semyanov@brain.riken.jp (A. Semyanov).
[1] These authors contributed equally to this work.

0143-4160/$ – see front matter © 2013 Elsevier Ltd. All rights reserved.
http://dx.doi.org/10.1016/j.ceca.2013.08.003

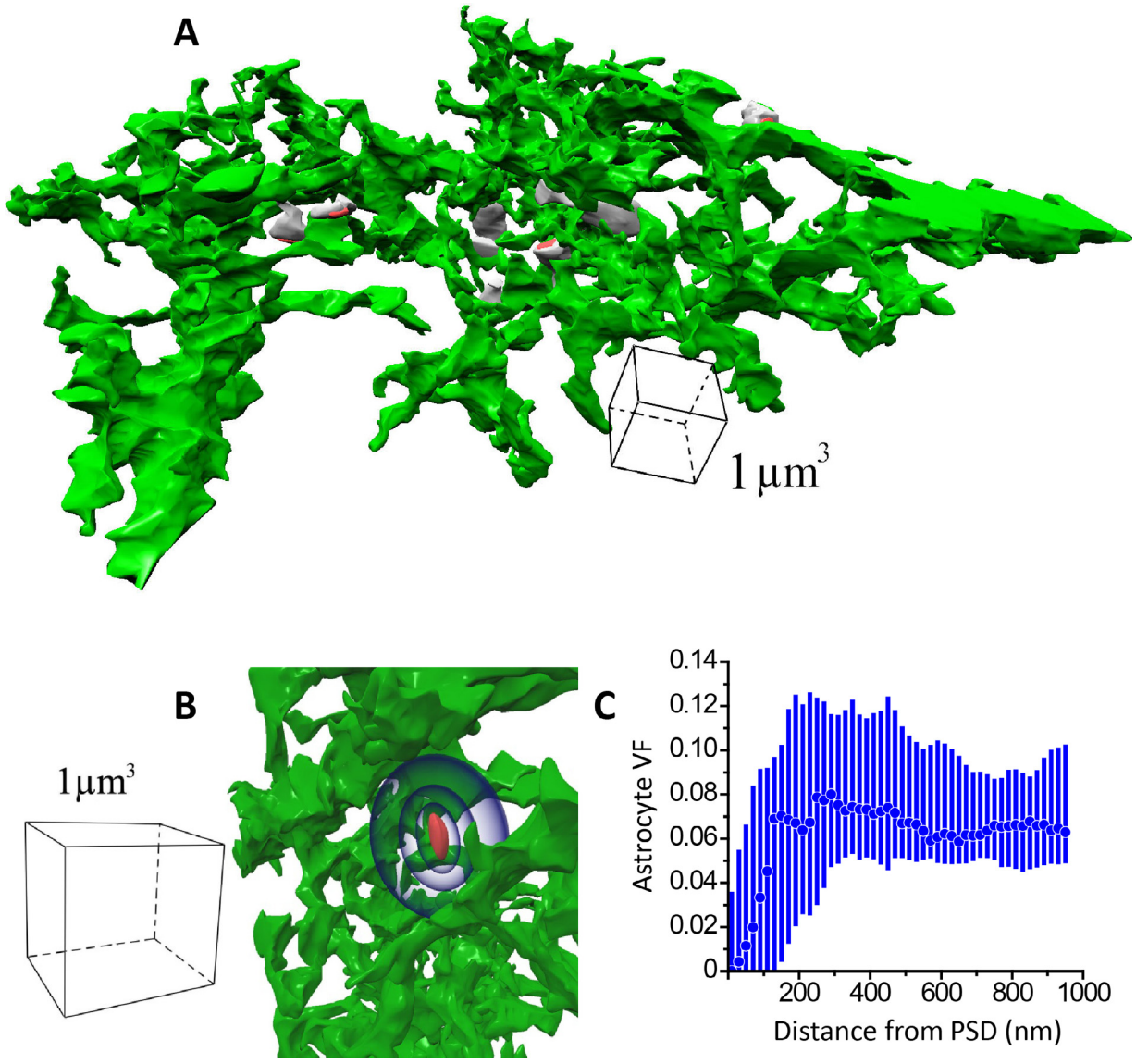

Fig. 1. Volume fraction occupied by astrocytic processes around synapses. (A) 3D reconstruction of the astrocytic processes (*green*) in the middle of the hippocampal CA1 *stratum radiatum*. Reconstruction of some typical spines (*gray*) with PSDs (*red*). (B) Magnified fragment of the astrocyte (*green*) centered around one of the PSDs (*red*) with equidistant surfaces plotted around it (*blue*). (C) Summary data of the astrocyte volume fraction (VF) versus the distance from the PSD. Box spans indicate lower and higher quartiles, circles – medians.

0.1 M Na-cacodylate buffer (pH 7.2–7.4) at room temperature. After perfusion, the brains were removed and 150-μm thick sections cut. The slices were further fixed for electron microscopy by immersion in 2.5% glutaraldehyde in the same 0.1 M Na-cacodylate buffer for 24 h. The tissue was postfixed with 1% osmium tetroxide and 0.01% potassium dichromate in the same buffer for 1–2 h at room temperature. Tissue was dehydrated in graded aqueous solutions of ethanol from 40% to 96% (each for 10 min) and then 100% acetone (three changes, each for 10 min). Specimens were infiltrated with a mixture of 50% epoxy resin and 50% pure acetone for 30 min at room temperature. Each slice was placed on an Aclar film and covered with a capsule containing pure epoxy resin (Epon 812/AralditeM epoxy resins) at 60 °C for 1 h and polymerized overnight at 80 °C. The embedded slices on the block surface were trimmed with a glass knife along the entire surface of the hippocampal slice and 1-μm thick sections were cut. A trapezoid area was prepared with a glass knife, with one side 250–350 μm in length, and included the CA1 hippocampal area. Serial sections (60–70 nm) were cut with a Diatome diamond knife and allowed to form a ribbon on the surface of a water/ethanol solution (2–5% ethanol in water) in the knife bath and collected using Pioloform-coated slot copper grids. Sections were counterstained with saturated ethanolic uranyl acetate, followed by lead citrate, and then placed in a rotating grid holder to allow for uniform orientation of sections on adjacent grids in the electron microscope. Serial sections in the middle of the *stratum radiatum* at a location 150–200 μm from the CA1 pyramidal cell body layer were obtained at a magnification of 6000× in a JEOL 1010 electron microscope (to assess the quality of EM data please see Supplementary image S1). Each image provided about 175 μm^2 for evaluation of dendritic, astrocyte, and axonal segments; different categories of synapses; PSDs; endoplasmic reticulum; and mitochondria. Up to 100 serial sections per series were photographed for reconstruction.

2.2. Tissue reconstruction

Electron microscope negatives were digitally scanned at a resolution of 1200 dpi. One of the series was chosen at random and a

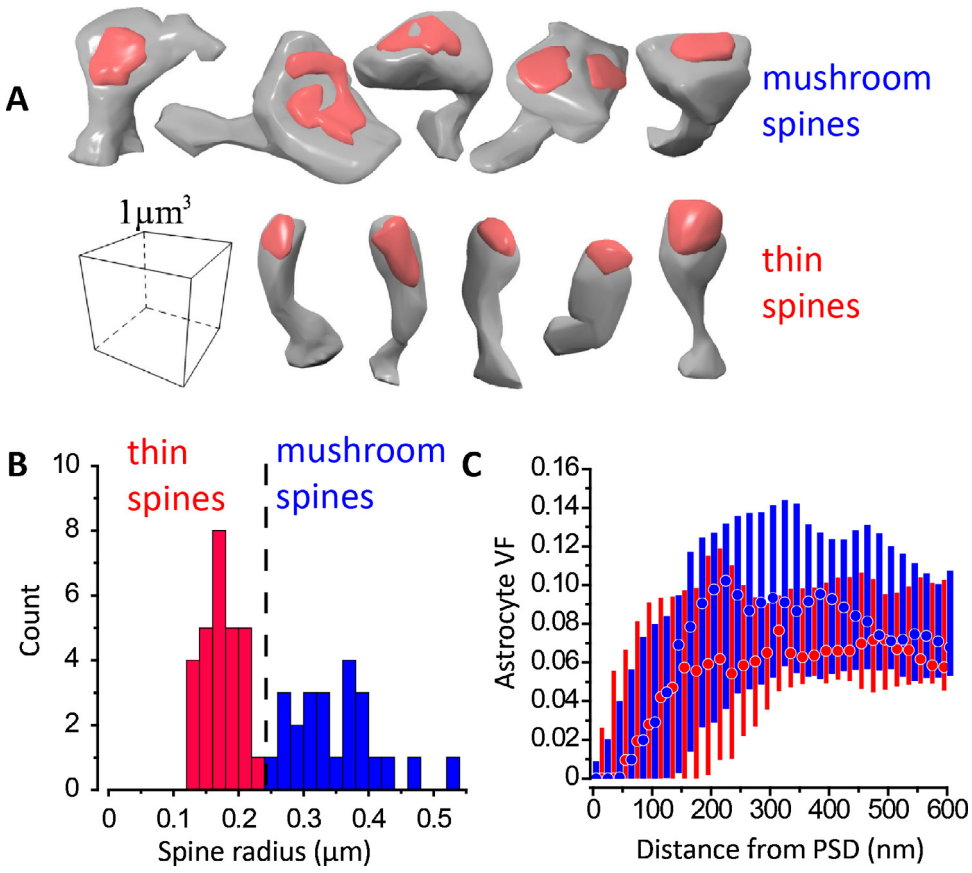

Fig. 2. Volume occupied by astrocytic processes varies between spine types. (A) Mushroom (*first row*) and thin (*second row*) spines. Mushroom spines have larger spine heads relatively to the neck and more complex form of PSD, sometime multiple PSDs. (B) Spines were divided into two groups according to the radiuses of their heads. (C) The astrocyte volume fraction, VF, was similar at short distances from the PSD, but then became significantly larger for mushroom spines. Box spans indicate lower and higher quartiles, circles – medians. (B and C) Blue color indicates mushroom spines and red indicates thin spines.

section in the series was aligned using homemade software. Cross-sectioned myelinated axons, mitochondria, and dendrites spanning each section provided a fiduciary reference for initial alignment of serial sections. Section thickness was determined using the approach of Fiala and Harris [21] and was normally 60–70 nm thick (gray-white color). Complete reconstruction of astrocyte processes, including endoplasmic reticulum, mitochondria, and 52 spines with PSDs was made inside a parallelepiped region. Contours of individual astrocyte processes, endoplasmic reticulum, mitochondria, spines, and PSDs were traced digitally, and the volumes, areas, and total numbers of structures were computed using Trace 1.26 (software developed by Dr. John Fiala [21] and available at http://synapses.bu.edu). 3D reconstructions were exported to 3DStudio Max software for rendering of final images.

2.3. Local SVR estimation on the astrocyte surface

SVR was calculated as a scalar field $SVR(X)$ in 3D space, where X is an arbitrary point on the surface of the astrocyte, which is the center of a secant sphere, Ω, with radius R (600 nm or 300 nm). $SVR(X)$ value was defined as follows:

$$SVR(X) = \frac{S}{V} \quad (1)$$

where S is the astrocyte surface area confined by the sphere Ω and V is the volume of the astrocyte confined by the sphere. S was calculated as a sum of the areas of the triangles entirely inside Ω and the areas of the parts of the triangles that are intersected by the sphere Ω. The sub-area of triangles intersected by Ω was calculated using the Monte Carlo method. V was estimated by integration of the surface thus increasing computational precision. The astrocyte surface represents a polygonal mesh comprising triangles $T_1, \ldots, T_n$ (n – number of triangles). For each triangle T_i, we calculated the value V_i using the Monte Carlo method. Then, V was obtained as the sum of V_i:

$$V = |V_1 + \cdots + V_n| \quad (2)$$

where $|V_i|$ is a volume bounded by triangle T_i and its projection from a point P chosen inside the sphere Ω.

To estimate a VF of the astrocyte or Ca^{2+} stores in an arbitrary point we also calculated the volume of the object inside the sphere Ω using the described method. For instance, to build the dependence between astrocyte SVR and Ca^{2+} stores fraction of astrocyte volume (Fig. 4A) we randomly took 5000 points on the astrocyte surface, and for each point calculated SVR and VF values using the sphere method. Knowing the distance to the nearest PSD for each point we obtained statistics, shown on Fig. 3B, D, etc.

2.4. Statistical data analysis

Statistical significance was tested using the Wilcoxon signed-rank test for all paired measurements and the Mann–Whitney test for all unpaired measurements using Origin 8 (OriginLab Corp.). The level of significance was set as $P < 0.05$. The group measures presented in the figures are expressed with box plots, indicating the quartiles where median is marked as ◯ or □. In the text, the data are given as mean ± standard error of the mean.

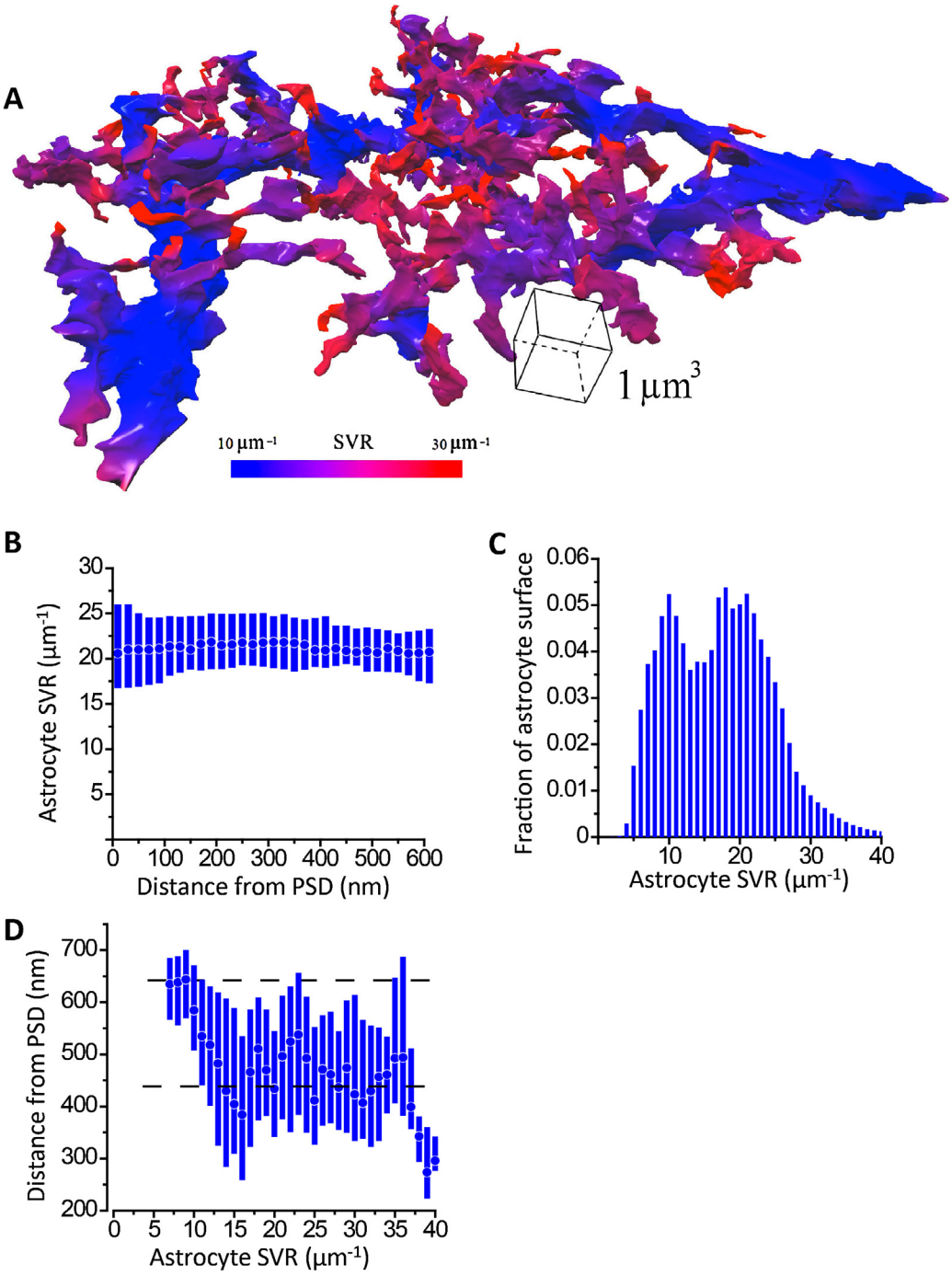

Fig. 3. Distribution of astrocyte SVR around PSDs. (A) 3D reconstruction of the astrocytic processes in the middle of the hippocampal CA1 *stratum radiatum* colored according to the SVR distribution. (B) Summary data of the astrocyte SVR versus the distance from the PSD. Box spans indicate lower and higher quartiles, circles–medians. (C) Surface distribution of the astrocyte SVR. (D) Summary data of distances from the PSD for the points on the astrocyte surface with different SVRs. Box spans indicate lower and higher quartiles, circles – medians.

3. Results

3.1. Volume fraction of astrocytic processes is largest between synapses

We investigated the ultrastructural properties of astrocytic processes at different distances from the postsynaptic density (PSD) using 3D reconstruction of serial electron microscope sections of the CA1 *stratum radiatum* (Fig. 1A and Video S1). Astrocytic coverage of the synapses was estimated as the proportion of the volume occupied by the astrocytes (volume fraction, VF) between equidistant surfaces around the PSD spaced in 20-nm increments (Fig. 1B). Mean astrocyte VF increased with an increase in the distance from the PSD edge, reaching a maximum around 250 nm (e.g., VF at a distance of 100 nm from the PSD: 0.056 ± 0.009 and at 250 nm: 0.081 ± 0.009, $n = 52$, $P < 0.001$, Wilcoxon signed rank test; Fig. 1C). Beyond 250 nm, the astrocyte VF did not change significantly with an increase in the distance from the PSD. Because the mean nearest-neighbor distance between synapses in the *stratum radiatum* of the rat hippocampus is approximately 500 nm [22], this finding

suggested that the highest astrocyte VF is reached in the middle between two synapses, providing a barrier to intersynaptic crosstalk. It is possible that most of the volume in the vicinity of the PSD is occupied by only the spine and the axonal varicosity. Alternatively, the astrocytes may maintain extra room around the PSD for its morphologic plasticity [12,13]. If astrocytic morphologic plasticity is associated with synaptic strength, the astrocyte VF would differ around different classes of synapses. Therefore, we measured the spine radius and detected two major groups of spines in the sample (according to the distribution and appearance): thin spines with mean radius $r = 179 \pm 7$ nm ($n = 20$) and mature mushroom spines with mean radius $r = 362 \pm 14$ nm ($n = 32$, Fig. 2A and B). Interestingly, both types of spines had a similar astrocyte VF at a 100-nm distance from the PSD (thin: 0.059 ± 0.013, $n = 20$ and mushroom: 0.052 ± 0.013, $n = 32$; $P = 0.94619$, Mann–Whitney test; Fig. 2C), suggesting that mean astrocytic coverage in the immediate proximity of the spine does not differ between spine types. At a distance of 250 nm, however, the astrocyte VF was significantly lower around thin spines (thin: 0.072 ± 0.01, $n = 32$ and mushroom: 0.095 ± 0.016; $n = 20$, $P = 0.03$, Mann–Whitney test), indicating a weaker barrier against intersynaptic crosstalk around thin spines. The division between thin and mushroom spines has functional relevance [23]. Mushroom spines comprise a stable population of spines that maintains traces of previous activity ('memory storage'), whereas thin spines comprise a plastic population of spines ('learning ready'). Thus, the lower spillover barrier around thin spines may be another feature that reflects their functional properties.

3.2. Astrocytic processes around synapses have a higher surface-to-volume ratio (SVR)

We then analyzed the distribution of SVR at different distances from the PSD. It is relatively easy to determine the SVR of an entire object, but calculating a local SVR is not trivial. To estimate the SVR distribution, we assigned an SVR to each point of the astrocyte surface. We used a secant sphere with a 600-nm radius centered at each point and identified the SVR of the process within this sphere (Fig. S2A). In this way, the entire astrocyte surface was mapped according to the local SVR (Fig. 3A). We then analyzed how the mean astrocyte SVR is distributed around the synapses. Surprisingly, the mean SVR was relatively independent of the distance from the PSD (SVR at 100 nm from the PSD: $20.95 \pm 0.88\ \mu m^{-1}$; at 250 nm: $21.38 \pm 0.78\ \mu m^{-1}$, $n = 52$, $P = 0.31$, Wilcoxon signed rank test; Fig. 3B). This finding, however, may reflect the size of the secant sphere ($r = 600$ nm), which could normalize the local differences in SVR. Therefore, we repeated the measurement using a sphere with smaller $r = 300$ nm and obtained a very similar SVR distribution, ruling out poor sensitivity of the method (Fig. S2B). Thus, astrocytic processes located around and between synapses have a similarly high SVR. If most of the astrocytic processes have a high SVR, however, they will contribute to a mean SVR with larger weight and may mask a contribution of the processes with a lower SVR. To test this, we determined the distribution of all astrocytic SVRs in the sample. The distribution showed two separate peaks at $10\ \mu m^{-1}$ and $19\ \mu m^{-1}$ suggesting presence of two distinct types of processes in the sample (Fig. 3C). Next, we analyzed mean distance from astrocytic processes with different SVRs to the nearest PSD (Fig. 3D). The results of this analysis indicated that processes with a lower SVR (first peak) were located further away from the PSDs than those with a higher SVR (distance to PSD from processes with $10\ \mu m^{-1}$ SVR: 587.21 ± 4.81 nm, $n = 52$; from processes with $19\ \mu m^{-1}$ SVR: 481.25 ± 4.24 nm, $n = 52$; $P = 0.26$, Wilcoxon signed rank test).

3.3. Ca^{2+} stores are located in astrocytic processes with a lower SVR

Next, we analyzed the distribution of Ca^{2+} stores in the astrocyte (Fig. S2 and Video S1). Ca^{2+} is stored in both the endoplasmic reticulum and mitochondria, but only a part of the mitochondrial volume is used for Ca^{2+} storage. Thus, we included the mitochondria in the VF of Ca^{2+} stores with a weight of 0.43 (experimentally estimated as a proportion of the intermembrane space). The VF of Ca^{2+} stores was larger in thick astrocyte processes with an SVR of $10\ \mu m^{-1}$ than in thin processes with an SVR of $19\ \mu m^{-1}$, which corresponds to PAPs (VF in thick processes: 0.114 ± 0.023, $n = 5000$; VF in thin processes: 0.016 ± 0.002, $n = 5000$, $P = 0.03$ Mann–Whitney test; Fig. 4A). This suggests that PAPs are practically devoid of Ca^{2+} stores which are concentrated in thick processes at a substantial distance from the PSD. To estimate this distance, we directly analyzed the distribution of Ca^{2+} stores at different distances from the PSD (Fig. 4B). We found that the VF of Ca^{2+} stores peaked at a mean distance of 1000 ± 325 nm ($n = 52$) from the PSD. This distance significantly varied from PSD to PSD (Fig. 4C); the peak was 'smoothed' in the relationship between VF of Ca^{2+} stores and distance from the PSD summarized for all PSDs (Fig. 4D). Therefore, we aligned the peak VFs of Ca^{2+} stores to determine the distribution of PAP lengths devoid of Ca^{2+} stores (mean: 542 ± 285 nm, $n = 52$; Fig. 4E). Thus, PAPs devoid of Ca^{2+} stores are longer than the estimated distance between synapses (500 nm).

4. Discussion

We developed an advanced geometrical method to assign the SVR to each point of the membrane surface, which allows for both mapping of the SVR along the entire process and analysis of its spatial distribution. This analysis demonstrated that the space between hippocampal CA1 synapses contains PAPs devoid of Ca^{2+} stores with a high SVR of around $19\ \mu m^{-1}$, while the processes containing Ca^{2+} stores with a lower SVR of around $10\ \mu m^{-1}$ are located at a greater distance from the synapses. This finding suggests morphologic specialization of the PAPs within tripartite synapses, similar to that of presynaptic axonal specialization (i.e., axonal varicosity) and postsynaptic dendritic specialization (i.e., dendritic spine). Such PAP specialization may be necessary for homeostatic function of the astrocyte. The high SVR of the PAPs increases the total surface of the astrocytic membrane within a small volume for better uptake of synaptically released neurotransmitters and K^+ [24]. A developmental origin of PAPs with a high SVR has been also proposed, i.e., when a tightly packed neuronal lattice is formed, glial cytoplasm simply fills empty spaces between preexisting neuronal elements [25]. This possibility is rather unlikely, however, because neurons can still find space to form proper dendritic spines in the adult brain [26–28]. Even newborn astrocytes and neurons can migrate from areas of neurogenesis in adult brain [29–31].

Thus, PAPs are optimized to maintain synaptic homeostasis, but do not serve as signaling compartments for store-dependent Ca^{2+} events. This, however, does not exclude the possibility that fast Ca^{2+} transients occur in PAPs in response to Ca^{2+} entry through the plasma membrane. Such Ca^{2+} entry can occur through (a) ligand activated channels (ionotropic glutamate receptors and P2X receptors), (b) transient receptor potential (TRP) channels and (c) operation of Na^+/Ca^{2+} exchanger (NCX) in reverse mode [32–36]. The latter is particularly interesting because glutamate/GABA uptake produces substantial increase in intracellular Na^+ [37] and thus NCX in astrocytes often operates in reverse mode bringing Ca^{2+} into the cytosol.

Astrocytic processes that contain Ca^{2+} stores and are therefore capable of IP_3-dependent Ca^{2+} release are located at a distance

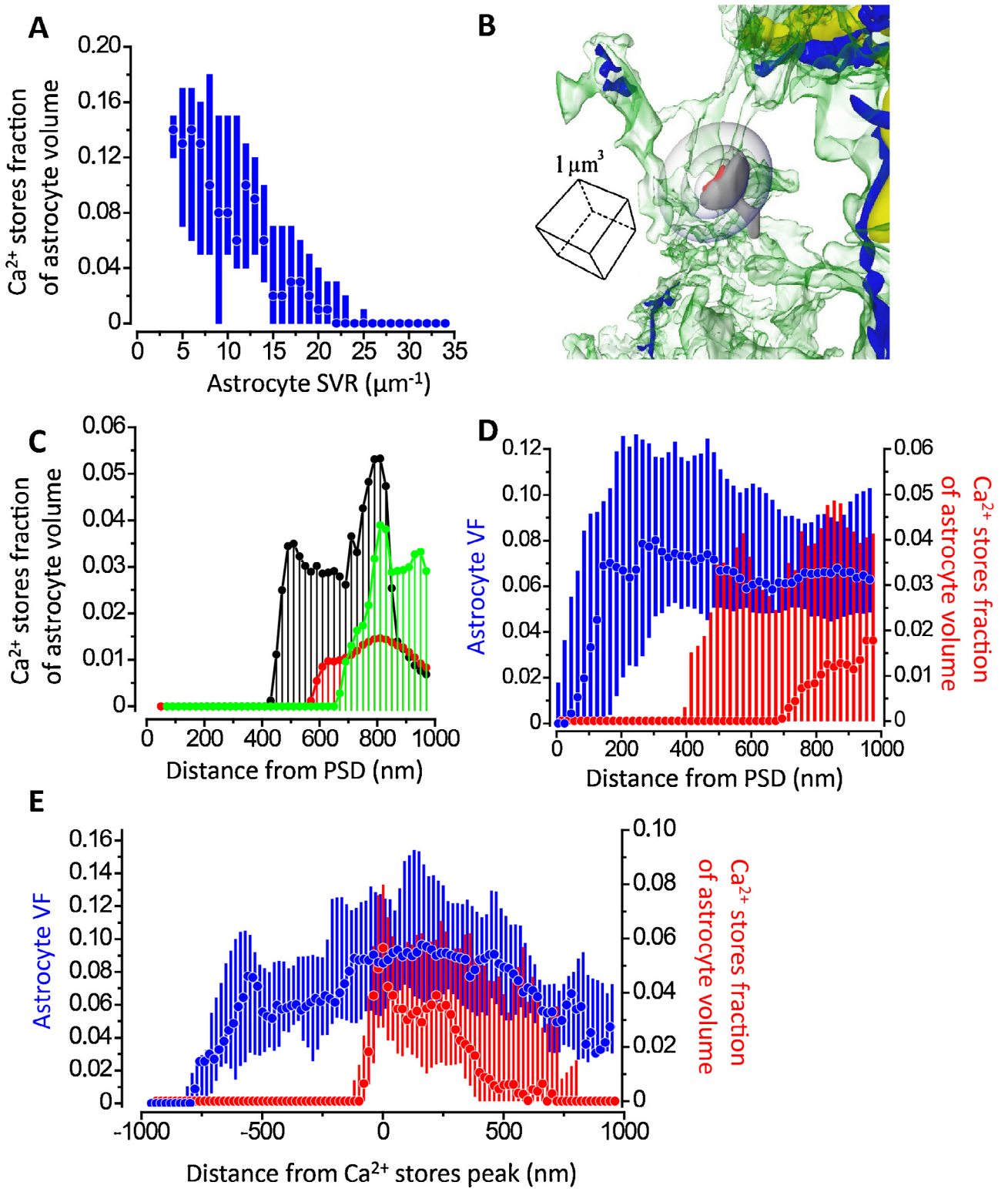

Fig. 4. Distribution of Ca^{2+} stores around PSDs. (A) Relationship between the fraction of astrocyte volume occupied by Ca^{2+} stores and astrocyte SVR. Box spans indicate lower and higher quartiles, circles – medians. (B) Magnified fragment of the astrocyte centered around one of PSDs (*red*) showing the location of Ca^{2+} stores (endoplasmic reticulum – *blue* and mitochondria – *yellow*). Equidistant surfaces plotted around PSD (*blue*) (C) Astrocyte volume occupied by Ca^{2+} stores versus distance from the PSD for 3 different PSDs (*green*, *red*, and *black* graphs). (D) Summary data of the fraction of astrocyte volume occupied by Ca^{2+} stores versus distance from the PSD (*red*) compared to the astrocyte volume fraction (*blue*) for all PSDs in the sample. Box spans indicate lower and higher quartiles, circles – medians. (E) Same as D, but the relationships for each PSD are centered on the Ca^{2+} stores peak (see also Fig. S2).

greater than the average intersynaptic distance from the synapses in the hippocampus [22]. This suggests that synapses are grouped together with PAPs at some distance from such 'active' processes, and indicates the possibility that in terms of Ca^{2+} store-mediated signaling astrocytes operate as integrators of local network activity, but not as detectors of individual synaptic events (Fig. S3).

The discovery of synaptic and extrasynaptic specialization of astrocytic processes raises several questions for discussion and

future studies. If Ca^{2+} events in astrocytes trigger the release of gliotransmitters (e.g., D-serine, glutamate, GABA), where does this release occur? The release can occur either extrasynaptically at 'active' processes or synaptically at PAPs where Ca^{2+} can diffuse from 'active' processes. In the first case, gliotransmission would be a mechanism regulating synaptic strength and plasticity in a local group of synapses [38,39]. In the second case, gliotransmission would participate in extrasynaptic communication in the brain (e.g., activation of extrasynaptic NMDA receptors [5,40], tonic $GABA_A$ conductance [41,42], etc.). We recently demonstrated that IP_3-dependent Ca^{2+} activity in astrocytes determines the degree of synapse coverage by PAPs [13]. When Ca^{2+} activity was reduced by astrocyte-specific expression of an IP_3 absorbent ('IP3 sponge'), the coverage of the synapses by PAPs was also reduced, promoting glutamate spillover. Taken together with the present data, this suggests a homeostatic feedback mechanism regulating the degree of synapse coverage by PAPs. When local network activity is low, reduced astrocytic Ca^{2+} dynamics decreases synaptic coverage by the astrocytes and 'opens the gates' for glutamate spillover. Elevated extrasynaptic glutamate concentrations enhance Ca^{2+} activity in astrocytes, thereby 'closing the gates'.

Finally, Ca^{2+} activity in astrocytes is a signal to brain vasculature regulating local blood flow [43]. It is reasonable that such signals are not triggered by individual synapses, but rather represent a response to the integrated activity of the local network, justifying the energy demand.

Acknowledgement

In memory of Dr. Victor Popov, who provided us with electron microscope serial images.

Appendix A. Supplementary data

Supplementary data associated with this article can be found, in the online version, at http://dx.doi.org/10.1016/j.ceca.2013.08.003.

References

[1] D.E. Bergles, C.E. Jahr, Glial contribution to glutamate uptake at Schaffer collateral–commissural synapses in the hippocampus, J. Neurosci. 18 (1998) 7709–7716.
[2] N.C. Danbolt, Glutamate uptake, Prog. Neurobiol. 65 (2001) 1–105.
[3] F. Asztely, G. Erdemli, D.M. Kullmann, Extrasynaptic glutamate spillover in the hippocampus: dependence on temperature and the role of active glutamate uptake, Neuron 18 (1997) 281–293.
[4] N. Lozovaya, S. Melnik, T. Tsintsadze, S. Grebenyuk, Y. Kirichok, O. Krishtal, Protective cap over CA1 synapses: extrasynaptic glutamate does not reach the postsynaptic density, Brain Res. 1011 (2004) 195–205.
[5] Y.W. Wu, S. Grebenyuk, T.J. McHugh, D.A. Rusakov, A. Semyanov, Backpropagating action potentials enable detection of extrasynaptic glutamate by NMDA receptors, Cell Rep. 1 (2012) 495–505.
[6] N.P. Poolos, M.D. Mauk, J.D. Kocsis, Activity-evoked increases in extracellular potassium modulate presynaptic excitability in the CA1 region of the hippocampus, J. Neurophysiol. 58 (1987) 404–416.
[7] D.E. Bergles, C.E. Jahr, Synaptic activation of glutamate transporters in hippocampal astrocytes, Neuron 19 (1997) 1297–1308.
[8] P. Kofuji, E.A. Newman, Potassium buffering in the central nervous system, Neuroscience 129 (2004) 1045–1056.
[9] M.R. Witcher, S.A. Kirov, K.M. Harris, Plasticity of perisynaptic astroglia during synaptogenesis in the mature rat hippocampus, Glia 55 (2007) 13–23.
[10] A. Araque, V. Parpura, R.P. Sanzgiri, P.G. Haydon, Tripartite synapses: glia, the unacknowledged partner, Trends Neurosci. 22 (1999) 208–215.
[11] G. Perea, M. Navarrete, A. Araque, Tripartite synapses: astrocytes process and control synaptic information, Trends Neurosci. 32 (2009) 421–431.
[12] D.T. Theodosis, D.A. Poulain, S.H. Oliet, Activity-dependent structural and functional plasticity of astrocyte–neuron interactions, Physiol. Rev. 88 (2008) 983–1008.
[13] M. Tanaka, P.Y. Shih, H. Gomi, T. Yoshida, J. Nakai, R. Ando, T. Furuichi, K. Mikoshiba, A. Semyanov, S. Itohara, Astrocytic Ca^{2+} signals are required for the functional integrity of tripartite synapses, Mol. Brain 6 (2013) 6.
[14] M.K. Shelton, K.D. McCarthy, Mature hippocampal astrocytes exhibit functional metabotropic and ionotropic glutamate receptors in situ, Glia 26 (1999) 1–11.
[15] J. Grosche, V. Matyash, T. Moller, A. Verkhratsky, A. Reichenbach, H. Kettenmann, Microdomains for neuron–glia interaction: parallel fiber signaling to Bergmann glial cells, Nat. Neurosci. 2 (1999) 139–143.
[16] X. Wang, N. Lou, Q. Xu, G.F. Tian, W.G. Peng, X. Han, J. Kang, T. Takano, M. Nedergaard, Astrocytic Ca^{2+} signaling evoked by sensory stimulation in vivo, Nat. Neurosci. 9 (2006) 816–823.
[17] G. Perea, A. Araque, Properties of synaptically evoked astrocyte calcium signal reveal synaptic information processing by astrocytes, J. Neurosci. 25 (2005) 2192–2203.
[18] W.J. Nett, S.H. Oloff, K.D. McCarthy, Hippocampal astrocytes in situ exhibit calcium oscillations that occur independent of neuronal activity, J. Neurophysiol. 87 (2002) 528–537.
[19] L. Pasti, A. Volterra, T. Pozzan, G. Carmignoto, Intracellular calcium oscillations in astrocytes: a highly plastic, bidirectional form of communication between neurons and astrocytes in situ, J. Neurosci. 17 (1997) 7817–7830.
[20] A. Reichenbach, A. Derouiche, F. Kirchhoff, Morphology and dynamics of perisynaptic glia, Brain Res. Rev. 63 (2010) 11–25.
[21] J.C. Fiala, K.M. Harris, Cylindrical diameters method for calibrating section thickness in serial electron microscopy, J. Microsc. 202 (2001) 468–472.
[22] D.A. Rusakov, D.M. Kullmann, Extrasynaptic glutamate diffusion in the hippocampus: ultrastructural constraints, uptake, and receptor activation, J. Neurosci. 18 (1998) 3158–3170.
[23] J. Bourne, K.M. Harris, Do thin spines learn to be mushroom spines that remember? Curr. Opin. Neurobiol. 17 (2007) 381–386.
[24] K.P. Lehre, D.A. Rusakov, Asymmetry of glia near central synapses favors presynaptically directed glutamate escape, Biophys. J. 83 (2002) 125–134.
[25] J. Grosche, H. Kettenmann, A. Reichenbach, Bergmann glial cells form distinct morphological structures to interact with cerebellar neurons, J. Neurosci. Res. 68 (2002) 138–149.
[26] P. Jourdain, K. Fukunaga, D. Muller, Calcium/calmodulin-dependent protein kinase II contributes to activity-dependent filopodia growth and spine formation, J. Neurosci. 23 (2003) 10645–10649.
[27] G.W. Knott, A. Holtmaat, L. Wilbrecht, E. Welker, K. Svoboda, Spine growth precedes synapse formation in the adult neocortex in vivo, Nat. Neurosci. 9 (2006) 1117–1124.
[28] M. Maletic-Savatic, R. Malinow, K. Svoboda, Rapid dendritic morphogenesis in CA1 hippocampal dendrites induced by synaptic activity, Science 283 (1999) 1923–1927.
[29] I.V. Kraev, O.V. Godukhin, I.V. Patrushev, H.A. Davies, V.I. Popov, M.G. Stewart, Partial kindling induces neurogenesis, activates astrocytes and alters synaptic morphology in the dentate gyrus of freely moving adult rats, Neuroscience 162 (2009) 254–267.
[30] N. Ohkawa, Y. Saitoh, E. Tokunaga, I. Nihonmatsu, F. Ozawa, A. Murayama, F. Shibata, T. Kitamura, K. Inokuchi, Spine formation pattern of adult-born neurons is differentially modulated by the induction timing and location of hippocampal plasticity, PLoS One 7 (2012) e45270.
[31] N. Toni, E.M. Teng, E.A. Bushong, J.B. Aimone, C. Zhao, A. Consiglio, H. van Praag, M.E. Martone, M.H. Ellisman, F.H. Gage, Synapse formation on neurons born in the adult hippocampus, Nat. Neurosci. 10 (2007) 727–734.
[32] O. Palygin, U. Lalo, A. Verkhratsky, Y. Pankratov, Ionotropic NMDA and P2X1/5 receptors mediate synaptically induced Ca^{2+} signalling in cortical astrocytes, Cell Calcium 48 (2010) 225–231.
[33] E. Shigetomi, X. Tong, K.Y. Kwan, D.P. Corey, B.S. Khakh, TRPA1 channels regulate astrocyte resting calcium and inhibitory synapse efficacy through GAT-3, Nat. Neurosci. 15 (2012) 70–80.
[34] D.A. Rusakov, K. Zheng, C. Henneberger, Astrocytes as regulators of synaptic function: a quest for the Ca^{2+} master key, Neuroscientist 17 (2011) 513–523.
[35] R.C. Reyes, A. Verkhratsky, V. Parpura, Plasmalemmal Na^+/Ca^{2+} exchanger modulates Ca^{2+}-dependent exocytotic release of glutamate from rat cortical astrocytes, ASN Neuro 4 (2012).
[36] R.C. Reyes, A. Verkhratsky, V. Parpura, TRPC1-mediated Ca(2+) and Na(+) signalling in astroglia: differential filtering of extracellular cations, Cell Calcium 54 (2013) 120–125.
[37] S. Kirischuk, V. Parpura, A. Verkhratsky, Sodium dynamics: another key to astroglial excitability? Trends Neurosci. 35 (2012) 497–506.
[38] S.Y. Gordleeva, S.V. Stasenko, A.V. Semyanov, A.E. Dityatev, V.B. Kazantsev, Bidirectional astrocytic regulation of neuronal activity within a network, Front Comput. Neurosci. 6 (2012) 92.
[39] C. Henneberger, T. Papouin, S.H. Oliet, D.A. Rusakov, Long-term potentiation depends on release of D-serine from astrocytes, Nature 463 (2010) 232–236.
[40] T. Papouin, L. Ladepeche, J. Ruel, S. Sacchi, M. Labasque, M. Hanini, L. Groc, L. Pollegioni, J.P. Mothet, S.H. Oliet, Synaptic and extrasynaptic NMDA receptors are gated by different endogenous coagonists, Cell 150 (2012) 633–646.
[41] M.C. Angulo, K. Le Meur, A.S. Kozlov, S. Charpak, E. Audinat, GABA, a forgotten gliotransmitter, Prog. Neurobiol. 86 (2008) 297–303.
[42] S. Lee, B.E. Yoon, K. Berglund, S.J. Oh, H. Park, H.S. Shin, G.J. Augustine, C.J. Lee, Channel-mediated tonic GABA release from glia, Science 330 (2010) 790–796.
[43] G.C. Petzold, V.N. Murthy, Role of astrocytes in neurovascular coupling, Neuron 71 (2011) 782–797.